Co-Fe Alloy/N-Doped Carbon Hollow Spheres Derived from Dual Metal-Organic Frameworks for Enhanced Electrocatalytic Oxygen Reduction

Song Lin Zhang, Bu Yuan Guan, and Xiong Wen (David) Lou**

[*] S. L. Zhang, Dr. B. Y. Guan, Prof. X. W. Lou

School of Chemical and Biomedical Engineering, Nanyang Technological University, 62 Nanyang Drive, Singapore, 637459, (Singapore)

Email: xwlou@ntu.edu.sg; davidlou88@gmail.com; Webpage: http://www.ntu.edu.sg/home/xwlou/

Abstract

Metal-organic framework (MOF) composites have recently been considered as promising precursors to derive advanced metal/carbon-based materials for various energy-related applications. Here, we develop a dual-MOF-assisted pyrolysis approach to synthesize Co-Fe alloy@N-doped carbon hollow spheres. Novel core-shell architectures consisting of polystyrene cores and Co-based MOF composite shells encapsulated with discrete Fe-based MOF nanocrystallites are first synthesized, followed by a thermal treatment to prepare hollow composite materials composed of Co-Fe alloy nanoparticles homogeneously distributed in porous N-doped carbon nanoshells. Benefitting from the unique structure and composition, the as-derived Co-Fe alloy@N-doped carbon hollow spheres exhibit enhanced electrocatalytic performance for oxygen reduction reaction. The present approach expands the toolbox for design and preparation of advanced MOF-derived functional materials for diverse applications.

Keywords: MOFs; hollow structures; Co-Fe alloy; N-doped carbon; oxygen reduction reaction.

Oxygen reduction reaction (ORR) is an important electrocatalytic reaction for metal-air batteries and fuel cells.[1-5] Nevertheless, the efficiency of these electrochemical devices has been constrained by the sluggish kinetics of the ORR. So far, platinum (Pt)-based materials have been considered as the most active catalysts for ORR.[6-8] However, the scalable application of the catalysts for ORR cannot be realized if expensive Pt-based catalysts are not replaced by other low-cost and high-performance electrode materials. Transition metal/N-doped carbon composite materials consisting of metal-nitrogen coordinated sites as catalytically active centers in carbon matrix have recently been considered as potential alternative electrocatalysts for ORR.[9-12] In particular, the electrocatalysts with multi-metal-nitrogen coordinated sites have been demonstrated to further promote their catalytic activity and selectivity.[13,14] In addition to the compositional control of the electrocatalysts, the enhancement of electrochemical performance can also be achieved by optimization of their nanostructures. Porous hollow particles with separated nanosized active sites and porous nanoshells have been widely used as nanoreactors in electrocatalysis. Apart from the shortened diffusion pathway for electrons/reactants, the discrete active sites in porous shells can also effectively prevent site overlap and thus increase the electrocatalytic activity and stability.[15-17] However, controllable synthesis of hollow structured multi-metallic alloy/N-doped carbon catalysts with separated nanosized active sites and porous carbon matrix towards high electrocatalytic performance still remains a great challenge, because of the difficulty in achieving relatively even distribution of multiple metal species in composite precursors and inhibiting the aggregation of the *in situ* formed alloy nanoparticles at high temperature.

In recent years, metal-organic frameworks (MOFs) have been regarded as promising precursors to derive metal/carbon-based functional materials for various energy-related applications.[18-20] Nevertheless, most MOFs-derived synthetic methods are based on simple MOF precursors.[21] As such, their derived metal/carbon-based composite materials often possess sole metal species and solid structures after thermal treatment under inert atmosphere.[22,23] Therefore, rational design and

preparation of relatively complex MOF composite precursors via the introduction of other MOFs or functional materials as co-precursors might be a suitable way for synthesis of hollow structured multi-metal/carbon-based electrocatalysts.[13,24]

Herein, we report a dual-MOF-assisted synthesis of Co-Fe alloy@N-doped carbon hollow spheres as an efficient electrocatalyst for ORR. Distinct from previous studies, the present synthetic approach relies on confined nanospace thermal transformation reaction of Fe-based MIL-101 nanoparticles in Co-based ZIF-67 nanoshell (**Figure 1**). The introduction of the second MOF nanoparticles into a MOF shell as co-precursor ensures evenly confined pyrolysis of MIL-101 nanocrystallites inside ZIF-67 nanoshell and easy production of small bimetallic Co-Fe alloy nanoparticles in N-doped carbon framework, which cannot be fabricated by direct pyrolysis of sole MIL-101 or ZIF-67. Benefiting from the rich catalytically active sites and porous conductive matrix, the as-prepared Co-Fe alloy@N-doped carbon hollow spheres manifest excellent electrocatalytic performance with enhanced activity and stability.

Monodisperse polystyrene (PS) spheres are synthesized through an emulsion polymerizing method (**Figure 2**a-c),[25] while another co-precursor MIL-101 nanocrystallites are prepared via a hydrothermal method (Figure 2d-f).[26] The surfaces of both PS spheres and MIL-101 nanoparticles are further functionalized with polyvinylpyrrolidone (PVP). The growth of MIL-101/ZIF-67 composite nanoshells on PS templates is conducted by adding MIL-101 nanoparticles, $Co(NO_3)_2$, and 2-methylimidazole (2-MIM) into the suspension of PS spheres. The dark purple PS@MIL-101/ZIF-67 product is produced after 2 hours at room temperature (Figure S1, Supporting Information). Field-emission scanning electron microscopy (FESEM) image reveals the morphology of the resultant PS@MIL-101/ZIF-67 spheres (Figure 2g). Uniform PS@MIL-101/ZIF-67 composite spheres are fully covered with MIL-101 nanocrystallites. Transmission electron microscopy (TEM) images show that PS@MIL-101/ZIF-67 core-shell spheres consist of many MIL-101 nanoparticles evenly distributed in the dual-MOF composite nanoshells (Figure 2h,i). As shown in the powder X-ray

diffraction (XRD) patterns, the PS@MIL-101/ZIF-67 composite spheres exhibit a similar diffraction pattern as ZIF-67 (Figure S2, Supporting Information). Compared with the diffraction peaks of ZIF-67, the unique peaks associated with MIL-101 at around 10^{o} are very weak, probably due to its low-degree crystallinity. Additionally, the existence of MIL-101 in the PS@MIL-101/ZIF-67 product is further demonstrated by energy-dispersive X-ray spectroscopy (EDX) measurement (Figure S3, Supporting Information). Besides, the density of MIL-101 nanocrystallites encapsulated in composite nanoshells and shell architecture can be finely tuned by adjusting the amount of MIL-101 nanocrystallites and concentration of Co^{2+} ions and 2-MIM added in the reaction system (Figure S4-S6, Supporting Information).

The Co-Fe alloy/N-doped carbon hollow spheres are fabricated via annealing treatment of the PS@MIL-101/ZIF-67 precursors at 700 ^{o}C under N_2 atmosphere. The pyrolysis product is denoted as Co-Fe/NC-700, where the number in the sample abbreviation represents pyrolysis temperature. The FESEM images of the Co-Fe/NC-700 spheres reveal that the sample maintains its original morphology after the annealing process (**Figure 3**a-c). The structure of the Co-Fe/NC-700 spheres is further elucidated by TEM image (Figure 3d). The hollow nanostructures are produced as the result of the decomposition of PS cores after the thermal treatment. Meanwhile, the Fe^{3+} and Co^{2+} ions in the dual-MOF shells are transformed to Co-Fe alloy nanoparticles, and the organic ligands in each MOF serve as nitrogen and carbon sources for the formation of N-doped carbon frameworks. Distinct from these Co-Fe alloy/N-doped carbon hollow spheres with well-defined structure, a mixture of aggregated Fe-Fe_3C large particles and carbon nanocages (Fe-Fe_3C/NC-700) as well as Co/N-doped carbon solid particles (Co/NC-700) are produced by direct pyrolysis of MIL-101 nanocrystallites and ZIF-67 polyhedra at 700 ^{o}C (Figure S7-S9, Supporting Information), respectively. Therefore, the encapsulation of MIL-101 nanocrystallites in the ZIF-67 nanoshell is not only essential to successfully produce bimetallic Co-Fe alloy through high-temperature transformation reaction, but also to realize the confined nanospace pyrolysis to form small alloy nanoparticles in carbon matrix.

The crystalline structure of the Co-Fe alloy is further determined by powder XRD analysis (Figure S10, Supporting Information). The diffraction pattern of the Co-Fe/NC-700 product is indexed to $Co_{0.7}Fe_{0.3}$ and $Co_{0.72}Fe_{0.28}$ alloy phases (JCPDS card No. 50-795 and 51-740). Closer examination on a Co-Fe/NC-700 hollow sphere shows the porous texture of the obtained nanoshell, which consists of many small Co-Fe alloy nanoparticles (Figure 3e,f). High-resolution TEM (HRTEM) image shows the lattice fringes of the alloy nanoparticles, which can be correlated to the (110) planes of $Co_{0.7}Fe_{0.3}$ alloy phase (Figure 3g). The selected area electron diffraction (SAED) pattern also verifies the alloy phase of the sample (Figure 3h). The EDX analysis reveals the existence of Fe, Co, C, and N elements in the pyrolysis product (Figure S11, Supporting Information). These elements are homogeneously distributed in the shells of Co-Fe/NC-700 hollow spheres (Figure 3i).

For comparison, Co-Fe/N-doped carbon samples with different crystalline phases are prepared by tuning the pyrolysis temperature from 600 ºC to 900 ºC. FESEM and TEM characterizations confirm that the Co-Fe/NC-600, Co-Fe/NC-800 and Co-Fe/NC-900 samples show similar features in morphology and structure as Co-Fe/NC-700 hollow spheres (Figure S12-S14, Supporting Information). The crystalline structure and composition for each composite material are further determined by XRD and X-ray photoelectron spectroscopy (XPS) analysis (**Figure 4**; Figure S15, Supporting Information). When the pyrolysis temperature is increased from 600 ºC, to 800 ºC, then to 900 ºC, the crystalline phase of the resultant products is varied from low-crystallinity Co/Fe species, to mixture of Co-Fe alloy, metallic Fe and Co, then to mixture of metallic Fe and Co (Figure 4a). XPS measurements further reveal the valence state and content of different elements in Co-Fe/NC products. Most Fe and Co elements in the Co-Fe/NC-600 sample exhibit high oxidation valence (Figure 4b,c), possibly due to incomplete reduction of metal species under low pyrolysis temperature of 600 ºC. When the temperature is further increased to 700 ºC, the amount of Fe and Co elements with high oxidation valence quickly decreases. Metallic Fe^0 and Co^0 become dominant, revealing the formation of Co-Fe alloy. By further increasing the temperature from 800 ºC to 900 ºC, the metallic

Fe^0 and Co^0 gradually decreases, possibly because of the inferior stability of the *in situ* formed metallic Fe and Co compared with alloy.[27] As the metal-nitrogen coordinated sites in the carbon matrix are the catalytically active centers of the electrocatalysts, the number of active centers strongly relies on N content for each sample.[28-31] The high-resolution N 1s spectra (Figure 4d) reveal the existence of four types of nitrogen species, pyridinic-N at ~398.7 eV, pyrrolic-N at ~400.1 eV, graphitic-N at ~401.1 eV and oxidic-N at ~403.2 eV. Among these Co-Fe/N-doped carbon composites, the Co-Fe/NC-700 sample exhibits higher N content than other three control samples.

The electrocatalytic activity of the Co-Fe/NC, Co/NC and Fe-Fe_3C/NC samples are investigated by rotating disk electrode (RDE) measurements in O_2-saturated KOH solution (**Figure 5**a). Both Co-Fe/NC-700 and Co-Fe/NC-800 samples consisting of Co-Fe alloy nanoparticles show superior ORR activity over the commercial Pt/C catalyst (20 wt.%; Johnson Matthey) in terms of half-wave potential (0.854 V and 0.842 V *vs.* 0.835 V). Compared with these catalysts with bimetallic alloy nanoparticles, Co-Fe/NC-900, Co-Fe/NC-600, Co/NC-700 and Fe-Fe_3C/NC-700 consisting of separated Co and/or Fe-based active sites manifest inferior half-wave potentials of 0.820 V, 0.787V, 0.808 V and 0.766 V (Figure 5a; Figure S16, Supporting Information), respectively. The improved electrocatalytic activity of bimetallic alloy catalysts might be attributed to the optimization of binding energy of O species via alloying Fe and Co in N-doped carbon matrix.[14] Of note, Co-Fe/NC-700 hollow spheres show similar Tafel slope as Pt/C catalyst, further confirming the remarkable electrocatalytic activity for the Co-Fe/NC-700 sample. RDE measurements at different rotating speeds from 100 to 2500 rpm are further used to study the electrocatalytic kinetics of the Co-Fe/NC-700 sample (Figure S17a, Supporting Information). The electron number (n) per O_2 involved in the ORR for the Co-Fe/NC-700 sample is calculated via the corresponding Koutecky-Levich (K-L) plots (Figure S17b, Supporting Information). The n value is determined to be about 3.81, suggesting that the oxygen reduction is dominated by the four-electron process. As the most active catalyst, the stability test of the Co-Fe/NC-700 sample is further examined via chronoamperometric response (Figure 5c). 97.7% of the original

current density is maintained for the Co-Fe/NC-700 electrode after 8 h, whereas the commercial Pt/C catalyst exhibits much higher current loss of 12.8%. The Co-Fe/NC-700 sample retains its structure and composition after stability test (Figure S18, Supporting Information). The Co-Fe/NC-700 sample and the commercial Pt/C catalyst are further compared by investigating the methanol crossover through chronoamperometric response. A significant reduction in the current density can be detected by the addition of methanol for the Pt/C catalyst, whereas the current density is not sensitive to the addition of methanol in the case of the Co-Fe/NC-700 catalyst (Figure 5d). The overall electrocatalytic performance of Co-Fe/NC-700 material is comparable to many metal/carbon-based electrocatalysts.[32-34]

Compared with other MOF-derived synthetic methods reported previously, this strategy employs dual-MOF precursors consisting of discrete Fe-based MIL-101 nanoparticles evenly encapsulated in Co-based ZIF-67 shells. Additionally, the nanospace-confined thermal transformation process guarantees even pyrolysis and conversion of Fe^{3+} and Co^{2+} ions in dual-MOF nanoshells to Co-Fe alloy, and prohibits excessive growth of active alloy nanoparticles in porous carbon matrix. The enhanced ORR performance of the Co-Fe alloy/N-doped carbon sample might be attributed to the following aspects. First, the bimetal-nitrogen coordinated active sites might grant high catalytic activity by optimizing the binding energy of O species through alloying Fe and Co.[14] Second, the sufficiently separated small Co-Fe alloy nanoparticles and N-doped carbon matrix render large active surface. Also, the porous structure and graphitic carbon effectively facilitate the mass/charge transport throughout these hollow particles, thus promoting the oxygen reduction process.

In summary, a dual-MOF-assisted pyrolysis approach is developed to synthesize Co-Fe alloy/N-doped carbon hollow spheres. The feature of this new approach is that each Co-base ZIF-67 nanoshell can effectively encapsulate many Fe-based MIL-101 nanocyrstallites. These PS@dual-MOF composite nanostructures can be converted into a hollow structured electrocatalyst consisting of separated Co-Fe alloy nanoparticles in the porous N-doped carbon framework. The as-prepared Co-

Fe alloy/N-doped carbon hollow spheres show enhanced electrocatalytic activity for oxygen reduction reaction compared with the catalysts consisting of separated Fe or/and Co species. This multi-MOF composite precursor approach can be applied for the design and construction of many other functional materials for different energy-related applications.

References

[1] A. C. Luntz, B. D. McCloskey, *Chem. Rev.*, **2014**, *114*, 11721-11750.

[2] Y. Li, H. Dai, *Chem. Soc. Rev.*, **2014**, *43*, 5257-5275.

[3] M. K. Debe, *Nature*, **2012**, *486*, 43.

[4] S. B. Adler, *Chem. Rev.*, **2004**, *104*, 4791-4844.

[5] Z. Chen, D. Higgins, A. Yu, L. Zhang, J. Zhang, *Energy Environ. Sci.*, **2011**, *4*, 3167-3192.

[6] Y. Nie, L. Li, Z. Wei, *Chem. Soc. Rev.*, **2015**, *44*, 2168-2201.

[7] C. Cui, L. Gan, M. Heggen, S. Rudi, P. Strasser, *Nat. Mater.*, **2013**, *12*, 765.

[8] A. Chen, P. Holt-Hindle, *Chem. Rev.*, **2010**, *110*, 3767-3804.

[9] Y. Jiao, Y. Zheng, M. Jaroniec, S. Z. Qiao, *Chem. Soc. Rev.*, **2015**, *44*, 2060-2086.

[10] R. Bashyam, P. Zelenay, *Nature*, **2006**, *443*, 63.

[11] K. Gong, F. Du, Z. Xia, M. Durstock, L. Dai, *Science*, **2009**, *323*, 760.

[12] W. Niu, L. Li, X. Liu, N. Wang, J. Liu, W. Zhou, Z. Tang, S. Chen, *J. Am. Chem. Soc.*, **2015**, *137*, 5555-5562.

[13] B. Y. Guan, Y. Lu, Y. Wang, M. Wu, X. W. Lou, *Adv. Funct. Mater.*, **2018**, *28*, 1706738.

[14] S. H. Noh, M. H. Seo, J. Kang, T. Okajima, B. Han, T. Ohsaka, *NPG Asia Mater.*, **2016**, *8*, e312.

[15] D. A. Proshlyakov, M. A. Pressler, C. DeMaso, J. F. Leykam, D. L. DeWitt, G. T. Babcock, *Science*, **2000**, *290*, 1588.

[16] N. R. Sahraie, U. I. Kramm, J. Steinberg, Y. Zhang, A. Thomas, T. Reier, J.-P. Paraknowitsch, P. Strasser, *Nat. Commun.*, **2015**, *6*, 8618.

[17] J. Liang, R. F. Zhou, X. M. Chen, Y. H. Tang, S. Z. Qiao, *Adv. Mater.*, **2014**, *26*, 6074-6079.

[18] B. Y. Xia, Y. Yan, N. Li, H. B. Wu, X. W. Lou, X. Wang, *Nat. Energy*, **2016**, *1*, 15006.

[19] H. Hu, L. Han, M. Yu, Z. Wang, X. W. Lou, *Energy Environ. Sci.*, **2016**, *9*, 107-111.

[20] B. Y. Guan, L. Yu, X. W. Lou, *Energy Environ. Sci.*, **2016**, *9*, 3092-3096.

[21] Y. V. Kaneti, J. Tang, R. R. Salunkhe, X. Jiang, A. Yu, K. C. W. Wu, Y. Yamauchi, *Adv. Mater.*, **2016**, *29*, 1604898.

[22] S. J. Yang, T. Kim, J. H. Im, Y. S. Kim, K. Lee, H. Jung, C. R. Park, *Chem. Mater.*, **2012**, *24*, 464-470.

[23] W. Xia, J. Zhu, W. Guo, L. An, D. Xia, R. Zou, *J. Mater. Chem. A*, **2014**, *2*, 11606-11613.

[24] B. Y. Guan, L. Yu, X. W. Lou, *Adv. Sci.*, **2017**, *4*, 1700247.

[25] J. Zhang, Z. Chen, Z. Wang, W. Zhang, N. Ming, *Mater. Lett.*, **2003**, *57*, 4466-4470.

[26] K. M. L. Taylor-Pashow, J. Della Rocca, Z. Xie, S. Tran, W. Lin, *J. Am. Chem. Soc.*, **2009**, *131*, 14261-14263.

[27] R. Ferrando, J. Jellinek, R. L. Johnston, *Chem. Rev.*, **2008**, *108*, 845-910.

[28] D. Guo, R. Shibuya, C. Akiba, S. Saji, T. Kondo, J. Nakamura, *Science*, **2016**, *351*, 361.

[29] B. P. Vinayan, S. Ramaprabhu, *Nanoscale*, **2013**, *5*, 5109-5118.

[30] L. Li, M. Shalom, Y. Zhao, J. Barrio, M. Antonietti, *J. Mater. Chem. A*, **2017**, *5*, 18502-18508.

[31] W. Wu, Q. Zhang, X. Wang, C. Han, X. Shao, Y. Wang, J. Liu, Z. Li, X. Lu, M. Wu, *ACS Catalysis*, **2017**, *7*, 7267-7273.

[32] Y. Zhao, K. Kamiya, K. Hashimoto, S. Nakanishi, *J. Phys. Chem. C*, **2015**, *119*, 2583-2588.

[33] R. Nandan, A. Gautam, K. K. Nanda, *J. Mater. Chem. A*, **2018**, *6*, 20411-20420.

[34] I. A. Khan, Y. Qian, A. Badshah, M. A. Nadeem, D. Zhao, *ACS Appl. Mater. Interfaces*, **2016**, *8*, 17268-17275.

Figures and captions

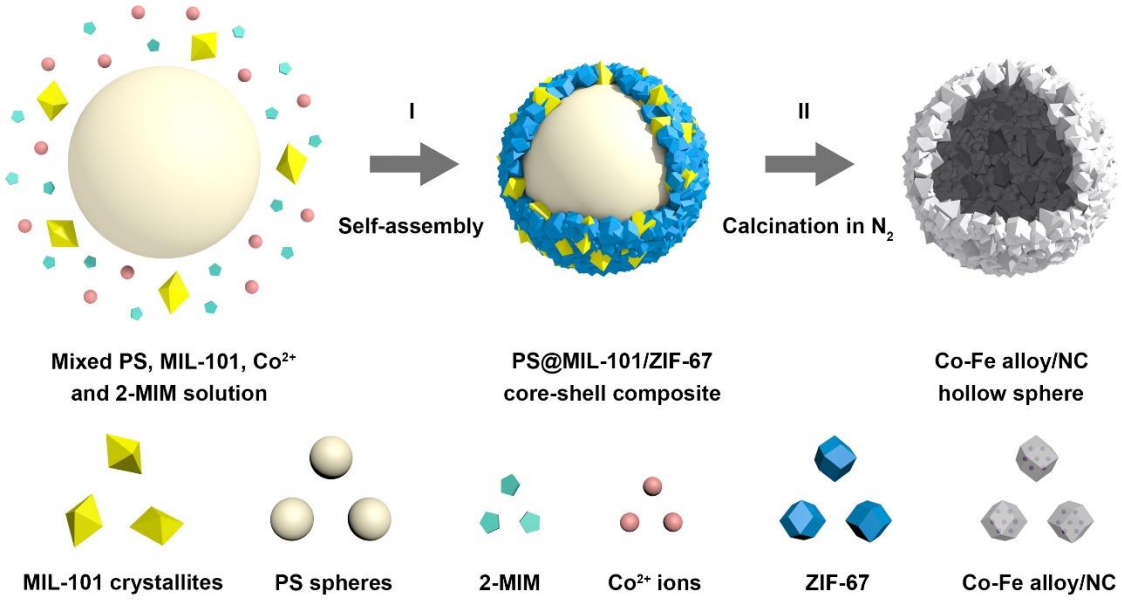

Figure 1. Schematic illustration of the formation process of Co-Fe alloy/N-doped carbon hollow spheres. PS@MIL-101/ZIF-67 core-shell composites are synthesized from coprecipitation of PS spheres, MIL-101 nanocrystallites and Co^{2+} ions in the presence of organic ligand 2-MIM. The PS@MIL-101/ZIF-67 core-shell composites are further converted to Co-Fe alloy/N-doped carbon hollow spheres via the annealing treatment under N_2 atmosphere.

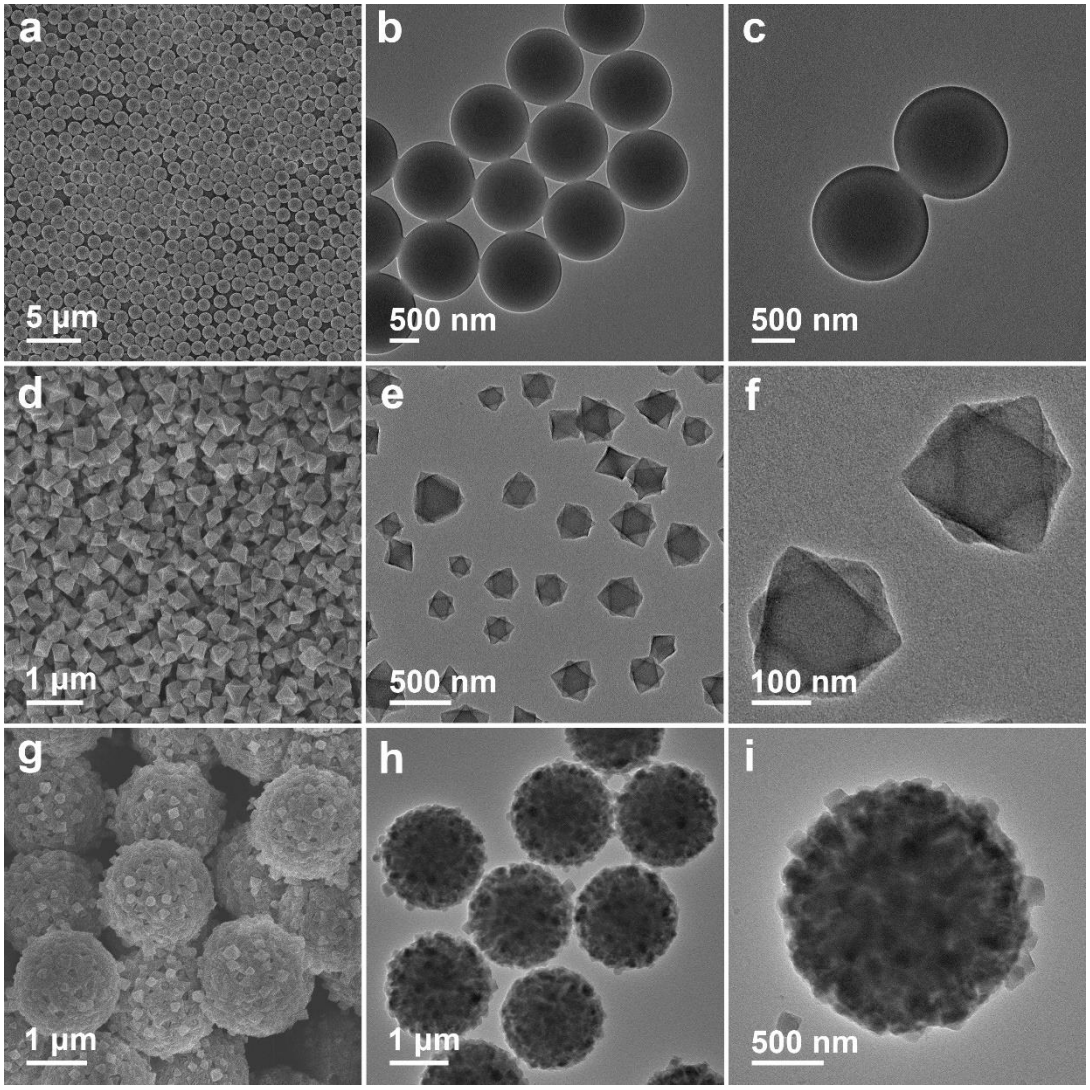

Figure 2. (a,d,g) FESEM and (b,c,e,f,h,i) TEM images of (a-c) PS spheres, (d-f) MIL-101 nanocrystallites, and (g-i) PS@MIL-101/ZIF-67 core-shell composites.

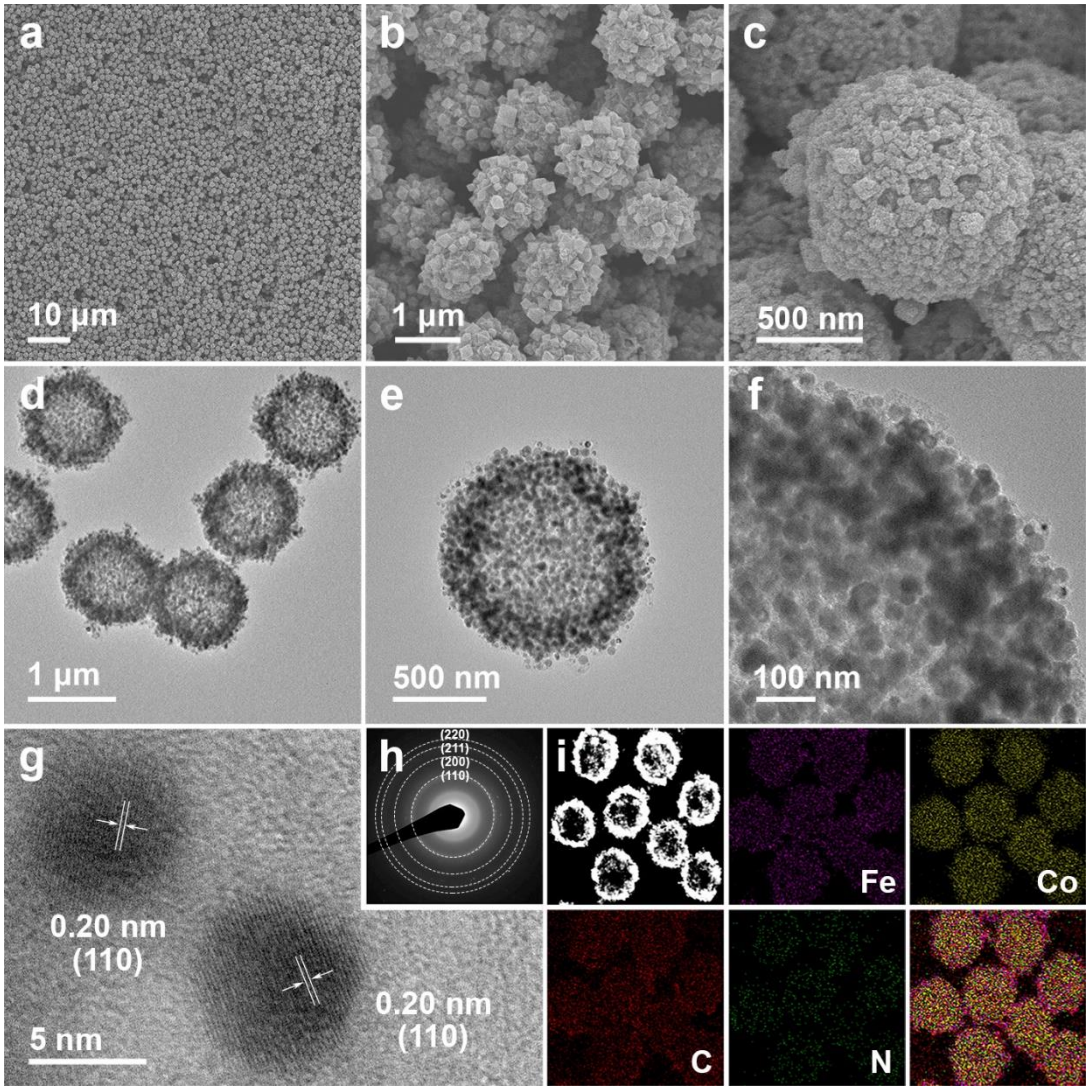

Figure 3. (a-c) FESEM images, (d-f) TEM images, (g) HRTEM image, (h) SAED pattern, and (i) HAADF-STEM and elemental mapping images of Co-Fe/NC-700 hollow spheres.

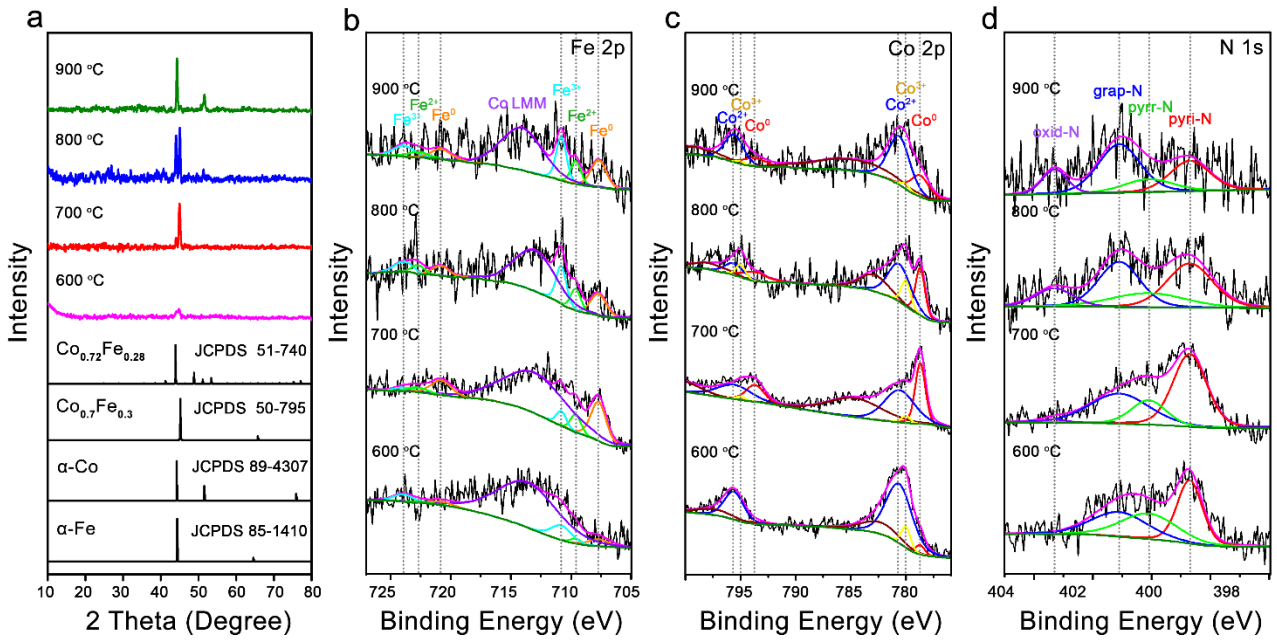

Figure 4. (a) XRD patterns and (b-d) XPS spectra of Co-Fe/N C composites prepared at different annealing temperatures of 600 ºC, 700 ºC, 800 ºC and 900 ºC. High-resolution spectra of (b) Fe 2p, (c) Co 2p and (d) N 1s.

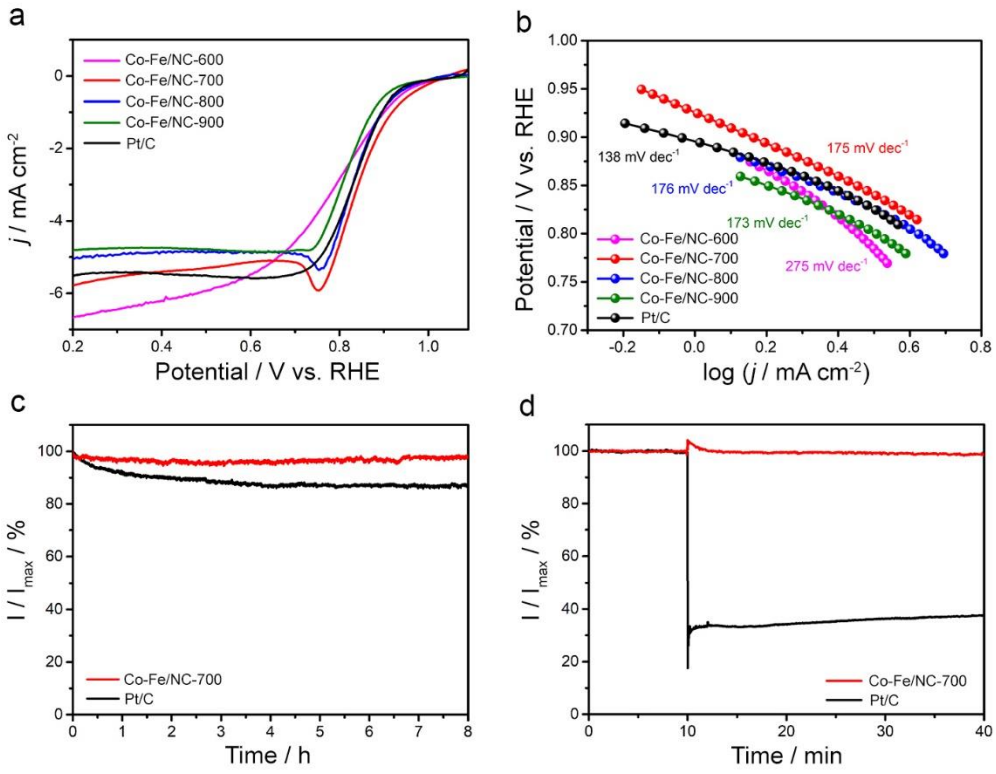

Figure 5. Electrocatalytic performance evaluation of Co-Fe/NC composites prepared at different annealing temperatures of 600 ºC, 700 ºC, 800 ºC and 900 ºC. (a) LSV curves in O_2-saturated 0.1 M KOH solution with a sweep rate of 10 mV s^{-1} at the rotating speed of 1600 rpm. (b) Tafel slope curves. (c) Chronoamperometric response at 0.5 V for 8 h. (d) Chronoamperometric response at 0.5 V after the introduction of 30 mL of methanol into 150 mL of 0.1 M KOH solution.

for Table of Content Entry

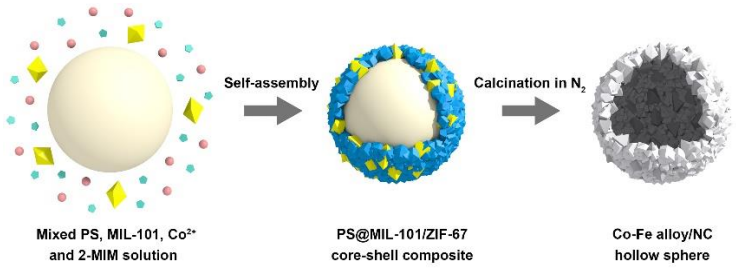

A dual-metal-organic-framework pyrolysis approach is developed to synthesize cobalt-iron alloy/nitrogen-doped carbon hollow spheres. With the structural and compositional advantages, these unique bimetallic alloy/carbon-based materials exhibit enhanced electrocatalytic performance for oxygen reduction reaction.